Chinese Chemical Letters 35 (2024) 108599

Contents lists available at ScienceDirect

Chinese Chemical Letters

journal homepage: www.elsevier.com/locate/cclet

Intermolecular hydrogen-bonding as a robust tool toward significantly improving the photothermal conversion efficiency of a NIR-II squaraine dye

Songtao Cai, Liuying Wu, Yuan Li, Soham Samanta, Jinying Wang, Bing Liu, Feihu Wu, Kaitao Lai, Yingchao Liu, Junle Qu, Zhigang Yang*

Center for Biomedical Photonics & Key Laboratory of Optoelectronic Devices and Systems of Ministry of Education and Guangdong Province, College of Physics and Optoelectronic Engineering, Shenzhen University, Shenzhen 518060, China

ARTICLE INFO

Article history:
Received 4 April 2023
Revised 18 May 2023
Accepted 21 May 2023
Available online 26 May 2023

Keywords:
Squaraine-based cyanine
Hydrogen bonds
High PCE
Anti-aggregation
Photothermal therapy

ABSTRACT

The photothermal therapy (PTT) has come across as a promising noninvasive therapeutic strategy for tumor treatment. However, low photothermal conversion efficiency (PCE) and hydrophobicity may impede the therapeutic efficacy of organic photothermal agents and an efficient PTT-agent must overcome these two major challenges. In this work, we developed a new strategy to promote higher PCE wherein the intermolecular hydrogen-bonding interaction between the single dye molecule and water facilitated the transformation of the absorbed energy into the heat. A hydrophilic squaraine dye (SCy1) with the second near-infrared region (NIR-II) absorption and extremely low emission were designed to exhibit much higher PCE than that of the analogues of pentamethine-dyes (PCy1, PCy2). The presence of the '$-O^{-}$' at middle of squaric cycle enabled the intermolecular H-bonding formation between the SCy1 and water to promote the energy dissipation channel. Moreover, the introduction of long-chain phenylsulfonate groups helped in to improve the water solubility apart from serving as an additional means of further enhancing PCE through fluorescence quenching. Therefore, SCy1 with a squaraine backbone and long-chain sulfonate moieties revealed outstanding photothermal stability and anti-aggregation activity apart from showing exceptionally high PCE (74%) in water. SCy1 demonstrated excellent therapeutic efficacy when applied in the PTT treatment of tumor-bearing mice under a laser irradiation of 915 nm.

In the field of cancer treatments, the photothermal therapy (PTT) has emerged as a reliable, noninvasive, remote-controllable therapeutic modality, in which the death of tumor cells is induced by the generation of local heat in the tumor tissue upon absorption of the external the near-infrared region (NIR) light energy [1,2]. Therefore, the therapeutic performance of a photothermal agent (PTA) is highly dependent on the photothermal conversion efficiency (PCE) wherein the PTAs with high PCEs usually result in the improved therapeutic efficacy. In the recent years, plenty of potential PTAs have been developed for PTT applications including organic/inorganic nanoparticles as well as organic small molecules [3–9]. However, organic small-molecule based PTAs are usually preferential than the organic/inorganic nanoparticles, since those can afford rapid clearance from the body and flexibility in design of smart probes apart from low-level systemic toxicity [10,11]. Especially, organic small molecular building blocks with NIR absorption (700–900 nm) and emission (1000–1700 nm) that can efficiently convert light energy into heat are regarded as the ideal photothermal agents since they can avoid the interference from the absorption of water in biological tissue [12–22].

Generally, in the PTT application, traditional single-molecular PTAs often encounter several shortcomings in terms of lower PCEs, weak photostability and/or poor solubility/biocompatibility, which ultimately jeopardize the overall therapeutic efficacy [23,24]. To address such issues, the hydrophobic PTAs are often encapsulated within the proteins or functional macromolecules, leading to the formation of polymers or nanostructures. For instances, encapsulating single-molecular PTAs such as indocyanine green (ICG) (PCE = ~3% for free molecules) in various macromolecules result in the improvements of PCE (PCE = ~9% and ~17% when encapsulated into the liposome and nanoparticles, respectively) [25,26]. However, such modifications may come up with the expense of other unsolicited issues such as higher toxicity and complex biological metabolism which are not desirable for any therapeutic treatment.

* Corresponding author.
E-mail address: zhgyang@szu.edu.cn (Z. Yang).

https://doi.org/10.1016/j.cclet.2023.108599
1001-8417/

An accessible alternative approach was presented by directly attaching the appropriate hydrophilic blocks to the single-molecular PTAs to modulate their water solubility, molecular weight, toxicity and clearance ability [15,27–31]. Nevertheless, in such cases, the PCE or photostability for single-molecular PTAs, remains very poor [22,32]. Generally, the organic small molecule probes prefer the non-radiative de-excitation pathways to endorse heat generation upon aggregation, which is favorable for PTT [27,33]. However, unsolicited excessive self-aggregation of PTAs may account for the poor performance in PTT treatments owing to the likely precipitation of PTAs. Therefore, the success of a PTT application is highly reliant on the availability of a reliable PTA wherein the rational designing of an apt single-molecule based PTA must adhere to the aforementioned considerations so that it can exhibit high PCE without compromising other qualities of a therapeutic agent. Therefore, it is highly significant yet challenging to develop new photostable single-molecule based PTA with NIR-II absorption, which can demonstrate robust PTT activity.

In this work, we have developed a new strategy to design single molecular PTAs with NIR-II absorption and high PCE wherein the intermolecular hydrogen-bonding interaction played a crucial role towards facilitating the transformation of the absorbed light energy into the heat. Two squaraine dyes (SCy1 and SCy2) and two cyanine dyes (PCy1 and PCy2) were synthesized to validate the rationality behind designing the probes, which are composed of similar backbones except the different conjugating chains (squaraine and pentamechine) (Scheme 1). All the dyes exhibited absorption and emission in the NIR-II regions in different solvents (>1000 nm); and squaraine-SCy1 and SCy2 possess extremely low fluorescence quantum yields (<0.0001), which is indicative of higher efficiency in converting light energy in the form of heat rather than emitting fluorescence. Typically, SCy1 is composed of both the squaric unit and phenylsulfonate moieties which played crucial roles in enhancing the PCE and increasing the aqueous solubility respectively. Therefore, the smart probe of SCy1 with high PCE was successfully applied in the PTT treatment of tumors which exhibited excellent positive therapeutic effect.

The multi-step synthetic routes for all the target squaraine dyes (SCy1, SCy2) and pentamethine dyes (PCy1, PCy2) from the starting material of 1–hydroxy-2-naphthaldehyde are illustrated in Scheme S1 (Supporting information). At first, the absorption properties of the dyes were studied using ultraviolet and visible (UV–vis) and NIR spectroscopy in organic solvents and aqueous solution. In organic solvents, all the dyes revealed prominent absorption maxima in the range of 880–910 nm while a minor absorption band was also present for each dye in the range of 790–820 nm (Fig. 1 and Fig. S1 in Supporting information). The red-shifted absorption peaks of each dye in the NIR region can be attributed to the presence of the extended π-conjugations. No major changes in spectral behaviors were recorded when the absorption properties of SCy1 and PCy1 were studied in aqueous medium. However, PCy2 revealed a broad, blue-shifted major absorption peak at 740 nm (Fig. 1b) in aqueous medium which can be attributed to its H-aggregation. The reference dyes (SCy2 and PCy2) that do not possess the sulfonate moieties revealed noticeable decrease of the absorption maxima in polar solvents (Figs. S2a, b and d in Supporting information) [30] may be due to the fact that in aprotic solvents their symmetric planar structures were retained which accounted for the strong absorption; whereas the planarity of the symmetric structures was somewhat lost in protic solvents like water, leading to the sharp decrease in their absorption. However, in SCy1 and PCy1, probably the integration of sulfonate moieties nullified the polarity-dependent variation in absorption bands to some extent as they lacked symmetric planar structures.

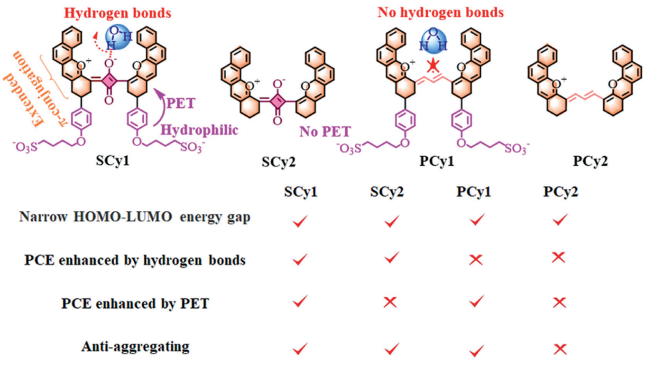

Scheme 1. Rational design of the high PCE NIR-II cyanine dye (SCy1, SCy2, PCy1 and PCy2) for PTT.

To verify whether the structural modifications, such as the presence of zwitterionic squaraine framework and the attachment of sulfonate moieties in the probe design, really played vital roles in improving the intermolecular H-bonding formation aptitude and aqueous solubility respectively or not, the concentration-dependent UV–vis absorption spectra of the dyes were measured. The concentration-dependent UV–vis spectra of SCy1, SCy2 and PCy1 in aqueous solution revealed that there is gradual increase in their absorbance peaks without any significant changes in the spectral behavior. However, incremental concentration PCy2 led to gradual increase in the blue-shifted absorbance maxima at 740 nm, indicating towards typical H-aggregate formation (Fig. S5 in Supporting information). The number of monomers units in the aggregates is determined as $n = 1$ for PCy2. It is important to mention that similar concentration-dependent absorption changes as well as H-aggregate formation were previously reported for common cyanine dyes (Fig. S6 in Supporting information) [34]. Probably the structural modifications with zwitterionic squaraine framework and/or the presence of sulfonate moieties in SCy1, SCy2 and PCy1 refrained them from showing such aggregation behavior (no H-aggregate formation). Meanwhile, light scattering grain size analysis further revealed that the hydration radius is 56 nm for PCy2, 1.5 nm for SCy2 and less than 1 nm for SCy1 and PCy1 (Fig. S7 in Supporting information). Therefore, the SCy1, SCy2 and PCy1 do not show excessive self-aggregation and can be studied in aqueous solution.

We also discussed the effect of the dynamic interaction of intermolecular hydrogen bond on the dyes with solvent molecules. In aprotic solvent of dimethoxyethylene (DME), the intrinsic absorption of SCy1 and SCy2 showed obviously blue-shifts after adding trifluoroacetic acid (TFA) (Fig. 1c, Figs. S8a and b in Supporting information), indicating the formation of the hydrogen bond between the squaraine scaffold in SCy1 or SCy2 and TFA. Blue shifts of 15 and 22 nm in the absorption peaks were observed for SCy1 and SCy2 respectively. In aqueous solutions, the addition of TFA caused rarely spectral variations of SCy1 and SCy2 (Figs. S9a and b in Supporting information), revealing the strong interaction between the dye molecules and water. However, the methine chains in PCy1 and PCy2 have no hydrogen bond formation sites. Therefore, the addition of TFA into DME or water solutions, resulted in the similar changes in the absorption behavior of PCy1 and PCy2 (causing a blue-shift (15, 12 nm) was observed from the absorption around 910 nm of in DME (Figs. S7c and S8c in Supporting information), meanwhile, PCy2 demonstrated typical disappear of aggregation in absorption spectra due to its improved solubility (Figs. S7d and S8d in Supporting information).

Subsequently, the fluorescence properties of all dyes were studied in detail using fluorescence spectroscopy. As shown in Fig. 1b and Fig. S1, the fluorescent spectra of all dyes revealed emission peaks larger than 1000 nm in dichloromethane (DCM). Unlike

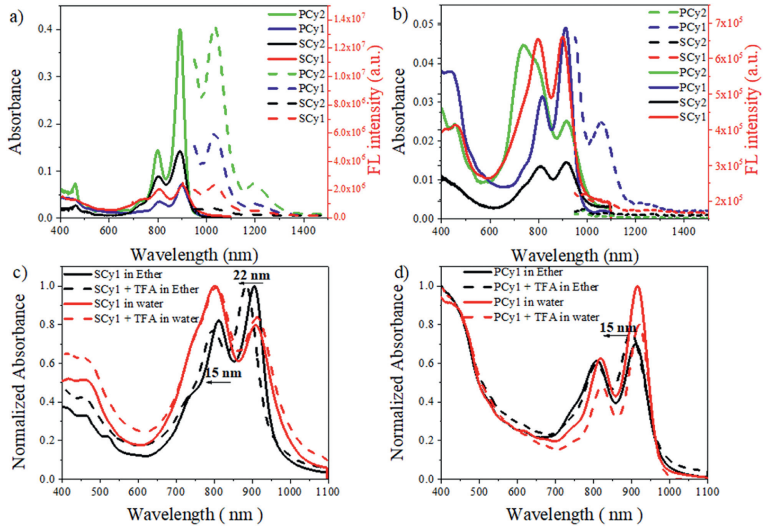

Fig. 1. The absorption (solid lines) and fluorescence (dotted lines) spectra of SCy1, SCy2, PCy1 and PCy2 (5 μmol/L) in (a) DCM and (b) H_2O. Normalized absorption spectra in DME and H_2O of SCy1 (c) and PCy1 (d) with addition of TFA or not.

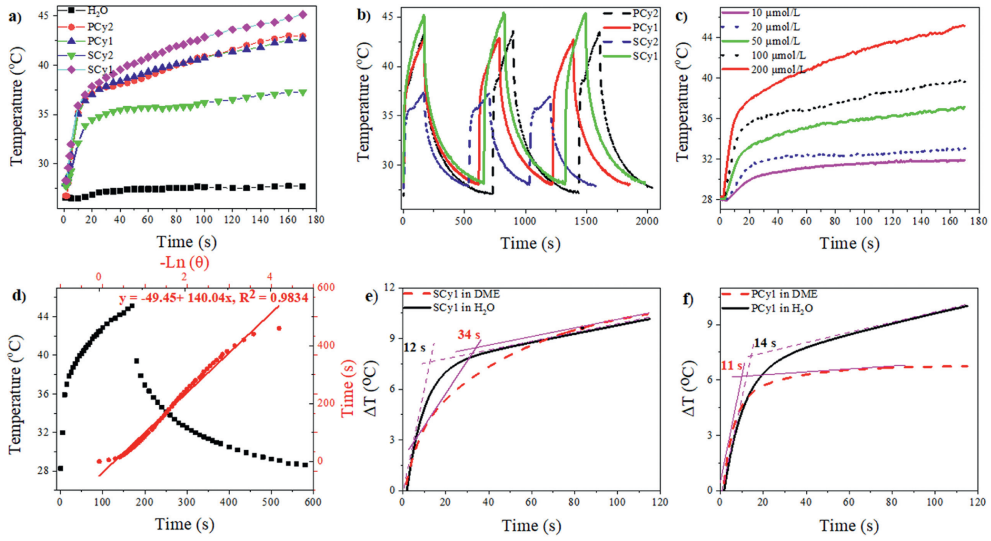

Fig. 2. (a) Temperature changes for H_2O, SCy1, SCy2, PCy1 and PCy2 (200 μmol/L) in water upon irradiation for 3 min (1.5 W/cm^2, 915 nm). (b) Curves showing the temperature change of SCy1, SCy2, PCy1 and PCy2 (200 μmol/L) in water over three ON/OFF cycles involving irradiation with a 915 nm laser (1.5 W/cm^2) for a period of time followed by passive cooling. (c) Temperature changes constant irradiation at 1.5 W/cm^2 with varying SCy1 concentrations (10, 20, 50, 100 and 200 μmol/L) in water. (d) Photothermal performance of SCy1 (200 μmol/L) by cooling to room temperature with linear analysis. (e, f) Temperature changes in DME and water of SCy1 and PCy1 (200 μmol/L, f) irradiation with a 915 nm laser (1.5 W/cm^2) for 120 s.

the classical cyanine dyes, each dye possessed Stokes shift over 100 nm, which indicated towards the poor co-planar rigidity and low fluorescence quantum efficiency. Even in organic solvents, the relative fluorescence quantum yield was lower than 0.0015 and negligible in water (<0.0001) (Tables S2–S5 in Supporting information). SCy1 revealed lowest fluorescence quantum yield, which suggests that the absorbed light energy was minimally released in the form of luminescence emission. We speculated that the rationally designed dyes such as SCy1 with extremely-low fluorescence quantum yield might exhibit interesting photothermal properties.

The photothermal performance of the dyes was assessed as new PTAs. As shown in Fig. 2a, in comparison with the pure water (which witnessed negligible change in temperature), all the probes experienced substantial increase in the temperature with exposure to the laser for 3 min. The noticeable, sharp temperature enhancement in a short span of time indicated that all probes exhibited reasonable PCE. Meanwhile, the dyes also displayed a concentration-dependent photothermal effect (Fig. 2c and Fig. S10 in Supporting information), apart from rendering strong resistance to photobleaching wherein the photothermal properties remained almost invariable even after three laser on-off (heating/cooling) cycles (Fig. 2b). This clearly indicated towards the decent photothermal stability of the dyes. The PCE values were evaluated for all probes from the corresponding temperature change in the heating/cooling processes, and SCy1, SCy2, PCy1 and PCy2 revealed the PCE values of 74.0%, 50.5%, 49.5% and 44.5%, respectively (Fig. 2d and Fig. S12 in Supporting information). As anticipated, squaraine-based dyes (SCy1, SCy2) exhibited higher PCEs than methine-based dyes (PCy1, PCy2), which further reiterated the role of hydrogen bond formation in the enhancement of PCE. Meanwhile, the PCE values of SCy1, SCy2, PCy1 and PCy2 (20.3%, 19.2%, 18.8% and 19.1%, respectively) in DME are much lower than that in water (Fig. S13 in Supporting information), which also validated that in case of squaraine dyes the scope of the dynamic interaction of intermolecular hydrogen bond with water became instrumental in enhancing the PCE in aqueous medium, whereas in the aprotic solvent of

DME, the lack of such dynamic intermolecular hydrogen bond interaction resulted in the lower PCEs. Besides, when exposed to the laser irradiation, the temperature of SCy1 and SCy2 in water tends to saturation within 15 s, while that in DME tends to saturation over 30 s. It basically indicated that the squaraine dyes (SCy1 and SCy2) can reveal significantly higher temperature increment rate upon NIR laser irradiation in water than in DME (Fig. 2e and Fig. S14a in Supporting information). In case of PCy1 and PCy2, negligible change in the temperature increment rate upon changing the solvent from H_2O (the time of temperature tends to saturation is 14 s for PCy1 and 15 s for PCy2) to DME (the time of temperature tends to saturation is 11 s for PCy1 and 17 s for PCy2) was observed as they structurally lacked dynamic intermolecular hydrogen bond interaction (Fig. 2f and Fig. S14b in Supporting information). Furthermore, SCy1, SCy2, PCy1 and PCy2 produced much less singlet oxygen (Fig. S15 in Supporting information) than classical PDT probes upon prolonged (15 min) laser exposure to reiterate that these dyes have much lower PDT efficiency [35]. Still, PCy1 and PCy2 have better ability to convert the absorbed light into singlet oxygen than SCy1 and SCy2 as confirmed by studying the absorption of 1,3-diphenylisobenzofuran (DPBF) within 6 min. Nevertheless, the produced singlet oxygen by either of the dyes is insufficient to cause marked PDT therapeutic effect. At the same time, SCy1, SCy2, PCy1 and PCy2 displayed good photostability wherein each dye revealed significant absorption even after 15 min laser irradiation (Fig. S15).

To further substantiate the contribution of the dynamic intermolecular hydrogen bonding formation between the dye and water molecule towards the enhancement of PCE, the corresponding theoretical calculations were also performed. When SCy1 was combined with water molecules, the single point energy of SCy1-b was found to be 5.3 kcal/mol and 12.9 kcal/mol lower than that of SCy1-c and SCy1-a, respectively (Fig. S16 in Supporting information). Meanwhile, the calculated results of absorption and emission properties of SCy1 and SCy1-b have been collected in Fig. S17, Tables S3 and S4 (Supporting information). The absorption and emission peaks of SCy1 and SCy1-b have some kind of hypsochromic shift with the water molecules addition (Table S3), which is in good agreement with the experimental data. The corresponding μ of SCy1-b decrease with the addition of water molecules (Table S4). Although the E_{ad} is larger, the k_r is slightly smaller. The reason is that the formation of hydrogen bonds results in larger distortion between squaraine and xanthene parts, which reduces the overlap between H and L. By contrast, the k_{ic} of SCy1-b is almost twice larger than that of SCy1 which lead to higher photothermal conversion efficiency of SCy1-b. For further exploration, the reorganization energies are calculated and analyzed. From Fig. 3, the total reorganization energies of SCy1 and SCy1-b are separately 495.81 and 521.09 cm^{-1}. With the addition of water molecules, the low-frequency (ω < 500 cm^{-1}) energy of SCy1 (107.64 cm^{-1}) is reduced to 88.70 cm^{-1}. However, the high-frequency (ω > 500 cm^{-1}) energy of SCy1 (388.17 cm^{-1}) is increased to 432.39 cm^{-1}. These data obviously indicate the contributions to total reorganization energies from dihedral angle is decreased and the bond stretch vibration make more contributions because of the suppression of SCy1's conformation from hydrogen bonds. Hence, the k_{ic} of SCy1-b is larger and the corresponding photothermal conversion efficiency is higher.

It is highlighted that in both SCy1 and PCy1 dyes, the introduction of the phenyl groups containing long-chain sulfonate moieties resulted in the enhancement in PCEs (PCE_{SCy1} > PCE_{SCy2} and PCE_{PCy1} > PCE_{PCy2}). This can be interpreted by the fact that the integration of the phenyl groups containing long-chain sulfonate moieties in SCy1 and PCy1 substantially quenched the fluorescence of the NIR-II fluorophores *via* PET mechanism (Fig. S16), which in turn increased their PCEs substantially since most of the absorbed energy (light) is then converted into heat in the presence of a squaraine structural backbone (capable of inducing favorable hydrogen bond formation) and insertion of phenyl group bearing sulfonate moieties (capable of increasing aqueous course of non-radiative decay. The rationally designed probe SCy1 possessing both the judicious structural amendments such as solubility and minimizing fluorescence output); revealed the highest PCE (74.0%) among the four synthesized probes. Therefore, SCy1 can be utilized as an excellent potential PTA andpotentially can be applied in PTT using low power light irradiation.

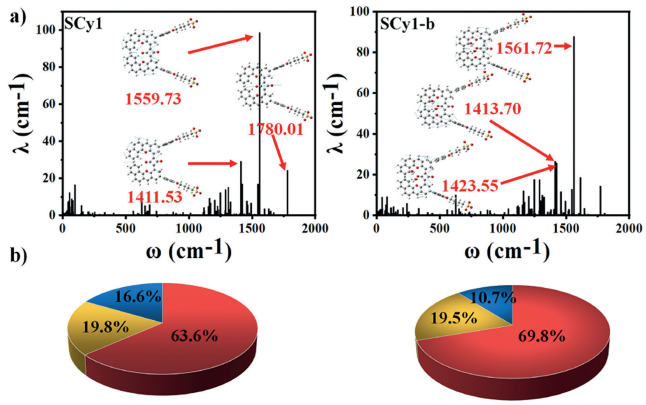

Fig. 3. (a) Calculated reorganization energies and crucial displacement vectors of the normal modes for SCy1 and SCy1-b in the DMSO. (b) Contributions to the total reorganization energies from bond length (red), bond angle (yellow) and dihedral angle (blue).

It is worth noting here that the smart probe of SCy1 revealed significantly higher PCE than many reported organic PTAs as compared in the Table S1 (Supporting information). The photothermal conversion aptitude of SCy1 was also tested in strong scattering environment like agarose (AGAR) gel with varying concentration to further optimize its PCE profile. As shown in Fig. S18a (Supporting information), when exposed to laser illumination, the temperature of SCy1 (100 μmol/L) agarose gel samples improved rapidly up to the temperature range (42–45 °C). It should be mentioned that the tumor tissues are more sensitive to hyperpyrexia in this temperature range (42–45 °C) than the normal tissues owing to the vascular inhomogeneity of the tumor site [36]. It was also noted that the excellent photothermal property of SCy1 can be repeated for more than 11 laser on-off heating/cooling cycles (Fig. S18b in Supporting information), which clearly indicated towards the high photothermal stability of SCy1. Therefore, excellent photothermal properties of SCy1 even in the strong scattering environment prompted us to study its potential applicability in the PTT treatment of tumor mice model.

Encouraged by the above results, SCy1, showing excellent PCE and reasonable photothermal stability was applied in the live *in vivo* PTT model to evaluate its therapeutic activity. Firstly, *in vitro* therapeutic efficacy of SCy1 was estimated by cell counting kit-8 (CCK-8) and live and dead cell viability assays, respectively. The probe SCy1 demonstrated the low cytotoxicity and the prominent phototoxicity (Fig. S19 in Supporting information). Then, the thermal effect SCy1 upon NIR laser irradiation in the *in vivo* mouse model was investigated. Animal welfare and experimental procedures have been reviewed and approved by the Animal Ethics Committee of Shenzhen University. As shown in Figs. 4a and b, when exposed to 915 nm laser, the temperature of mouse hindlimb, injected subcutaneously with SCy1 was seen to be elevated rapidly up to over 42 °C within 1 min. It was interesting to note that the increase in the temperature had a direct correlation with the concentration of the potential PTA, SCy1. For instance, the temperature increased from 36.7 °C to 42.7 °C when

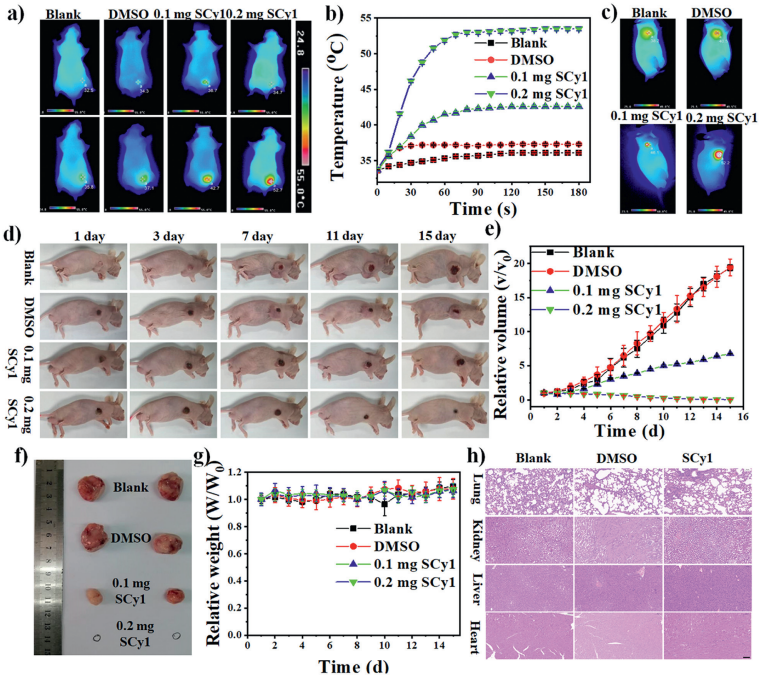

Fig. 4. (a) The IR thermal imaging of the normal mouse and the mouse injected subcutaneously with DMSO and SCy1 under laser irradiation (915 nm, 1.2 W/cm^2) for 3 min. (b) Temperature varies with irradiation time of laser (915 nm, 1.2 W/cm^2), which is the reflection of data from (a). (c) The IR thermal images of the normal mouse and the mouse injected subcutaneously with DMSO and SCy1 after exposed to laser (915 nm, 1.2 W/cm^2) for 3 min. (d) Images of one mouse from blank group and the mouse injected with DMSO and SCy1 group at the 1th, 3th, 7th, 11th and 15th day after PTT (915 nm, 1.2 W/cm^2, 3 min). (e) Tumor growth curves of mice in different groups after PTT (mean ± standard deviation, $n = 5$). (f) Tumor images of two mice from each group at 15 d after PTT. (g) Mice body weight variation with post-treatment time in different treatment groups (mean ± standard deviation, $n = 5$). (h) H&E analysis of the major organs collected from blank, DMSO, and SCy1 (0.2 mg) at the end of the treatment (scale bar: 100 μm).

0.1 mg SCy1 was administered whereas upon injecting 0.2 mg SCy1 there was much steady increase in the temperature from 34.7 °C to 52.7 °C (the laser power and other variables remain constant). On the contrary, laser irradiation to the mouse without injecting the SCy1 probe or the only DMSO treated mouse, witnessed negligible increase in the temperature range which cannot be considered for treating tumor cells. Therefore, the rationally designed squaraine dye SCy1 can act as a potential PTA to effectively generate heat in the tumor environment upon laser irradiation which is adequate for inducing tumor hyperthermia and hence, can be used in PTT for the effective treatment of tumors.

To further verify the therapeutic efficacy of SCy1 in PTT, the ability of SCy1 was evaluated as an anti-tumor growth agent in 4T1 tumor-bearing mice. To perform the experiment, tumor-carrying mice were randomly classified into four groups: blank (only mice), DMSO, 0.1 mg SCy1 and 0.2 mg SCy1. DMSO, 0.1 mg SCy1 and 0.2 mg SCy1 were individually delivered to the tumor tissue by subcutaneous injection at tumor site. The four groups of mice were then continuously irradiated with laser exposure for 3 min. The photothermal therapeutic capability was evaluated through monitoring the tumor volumes in each case for 15 days. As displayed in Fig. 4c, the temperature of the SCy1-treated mice increased to 46.1 and 52.2 °C after irradiated with laser for 3 min, while the final temperature of the "Blank" and "DMSO" mouse is 38.2 and 40.5 °C, respectively, indicating a high hyperthermia therapeutic efficacy of SCy1 *in vivo*. Meanwhile, the "Blank" and "DMSO" mice groups witnessed a steady increase the tumor volume, while the tumor volume was significantly reduced in the "0.1 mg SCy1" group. However, in "0.2 mg SCy1" group, the tumor was almost eliminated (Figs. 4d and e). The dissected tumor in each case upon the potential PTT treatment has been depicted in Fig. 4f with volume measurement to further represent the PTT activity of SCy1. These results, not only reaffirmed the remarkable therapeutic efficacy of SCy1 as a robust PTA towards effective cure of tumor using PTT, but also highlighted the need for standardizing the effective dose of administering SCy1.

To verify whether the single-molecule SCy1 can be rapidly metabolized *in vivo* or not, the PTT effect of 4T1 tumor-bearing mice, injected intravenously with SCy1 was carefully evaluated. At first, the IR thermal images of 4T1 tumor-bearing mice, injected intravenously with DMSO and SCy1 were measured to evaluate the distribution. As shown in Fig. S20 (Supporting information), the normal mouse (36.7 °C) and the mouse injected intravenously with DMSO and SCy1 (~35.4 °C) could not reveal significant increase in the temperature at tumor site (<37 °C) under the laser irradiation even after 24 h post injection. Meanwhile, the "DMSO" and "0.2 mg SCy1" mice groups witnessed a steady increase of the tumor volume within 15 days after treatment as depicted in Fig. S21b (Supporting information). The mice were later sacrificed and the tumor was dissected for capturing photograph (Fig. S21c in Supporting information). It was confirmed that SCy1 injected intravenously fails to accumulate in the tumor and hence could not produce the effective therapeutic effect which indicated towards the easy *in vivo* clearance aptitude of SCy1.

Moreover, the mice, which administered with SCy1 subcutaneously and intravenously, showed negligible alternation in the body weight throughout the course of PTT treatment studies (Fig. 4g and Fig. S21d in Supporting information), and H&E stains of the main organs were examined and demonstrated that the SCy1 has no discernible damage on normal tissues (Fig. 4h and Fig. S22 in Supporting information). So, the excellent biocompatibility and *in vivo* adaptability of SCy1 was confirmed. Such highly effective suppression of tumor growth using SCy1 in the *in vivo* PTT experiment suggests that the rationally designed SCy1 can also be applied as a robust photo-thermal agent for treating tumor in other advanced animal models.

In conclusion, the squaraine-based cyanine dyes (SCy1 and SCy2) and methine-based cyanine dyes (PCy1 and PCy2) with NIR-II absorption and emission were judiciously designed and synthesized to evaluate their potential as effective photothermal agents. The squaraine-based cyanine dye SCy1 which possessed both the squaraine structural framework capable of enhancing the PCE *via* hydrogen bond formation as well as insertion of phenyl-bearing long chain sulfonate inducing better aqueous solubility and fluorescence quenching revealed excellent PCE (as high as up to 74%) and good photothermal stability which is far superior than most of the reported PTAs. Therefore, SCy1 was applied as a potential PTA in cancer treatment after optimizing the most effective concentration range which revealed that it can yield outstanding therapeutic outcome in the *in vivo* mice model. The presented new probe designing strategy not only deliberated upon certain crucial structural amendments that could leverage many important features like hydrogen bond formation, aqueous solubility and fluorescence quenching to bring noticeable improvement in PCE but also helped in to develop a new biocompatible PTA like SCy1 that showed robust therapeutic performance in the *in vivo* mice model towards possible cure of cancer.

Declaration of competing interest

The authors declare that they have no known competing financial interests or personal relationships that could have appeared to influence the work reported in this paper.

Acknowledgments

This work was financially supported by the National Natural Science Foundation of China (No. 61875131). Shenzhen Key Laboratory of Photonics and Biophotonics (No. ZDSYS20210623092006020). Thank Prof. Jian Wang (Institute of Theoretical Chemistry, Jilin University) for the help of theoretical calculation.

Supplementary materials

Supplementary material associated with this article can be found, in the online version, at doi:10.1016/j.cclet.2023.108599.

References

[1] K. Li, M. Lu, X. Xia, Y. Huang, Chin. Chem. Lett. 32 (2021) 1010–1016.
[2] H.S. Jung, P. Verwilst, A. Sharma, et al., Chem. Soc. Rev. 47 (2018) 2280–2297.
[3] A.J. McGrath, Y. Chien, S. Cheong, et al., ACS Nano 9 (2015) 12283–12291.
[4] B. Zhang, H. Wang, S. Shen, et al., Biomaterials 79 (2016) 46–55.
[5] D. Zhang, H. Xu, X. Zhang, et al., ACS Appl. Mater. Interfaces 10 (2018) 25203–25212.
[6] K. Wang, Y. Xiang, W. Pan, et al., Chin. Chem. Lett. 33 (2022) 793–797.
[7] C. Ye, S. Zhang, D. Zhang, et al., Chin. Chem. Lett. 34 (2023) 108223.
[8] Q. Zou, M. Abbas, L. Zhao, et al., J. Am. Chem. Soc. 139 (2017) 1921–1927.
[9] R. Chang, Q. Zou, L. Zhao, et al., Adv. Mater. 34 (2022) 2200139.
[10] W. Feng, W. Zhao, Z. Chen, et al., ACS Appl. Bio Mater. 3 (2020) 5722–5729.
[11] S. Liu, X. Zhou, H. Zhang, et al., J. Am. Chem. Soc. 41 (2019) 5359–5368.
[12] S. Zhu, R. Tian, A.L. Antaris, X. Chen, H. Dai, Adv. Mater. 31 (2019) 1900321.
[13] B. Zhou, Y. Li, G. Niu, et al., Appl. Mater. Interface. 8 (2016) 29899–29905.
[14] Y. Zhang, M. Zhao, J. Fang, et al., ACS Appl. Mater. Interfaces 13 (2021) 12857–12865.
[15] H. Qian, Q. Cheng, Y. Tian, et al., J. Mater. Chem. B 9 (2021) 2688–2696.
[16] F. Li, T. Li, D. Zhi, et al., Biomaterials 256 (2020) 120219.
[17] D. Yao, Y. Wang, R. Zou, et al., ACS Appl. Mater. Interfaces 12 (2020) 4276–4284.
[18] P. Sun, Q. Wu, X. Sun, et al., Chem. Commun. 54 (2018) 13395–13398.
[19] Y. Li, J. Zhang, S. Liu, et al., Adv. Funct. Mater. 31 (2021) 2102213.
[20] J. Li, R. Wang, Y. Sun, et al., ACS Appl. Mater. Interfaces 13 (2021) 54830–54839.
[21] Y. Zheng, Q. Li, J. Wu, et al., Chem. Sci. 12 (2021) 1843–1850.
[22] Y. Wang, G. Xia, M. Tan, et al., Adv. Funct. Mater. 32 (2022) 2113098.
[23] Y. Zou, M. Li, T. Xiong, et al., Small 16 (2020) 1907677.
[24] H.S. Jung, J. Lee, K. Kim, et al., J. Am. Chem. Soc. 139 (2017) 9972–9978.
[25] H. Yoon, H. Lee, J. Lim, J. Park, ACS Appl. Mater. Interfaces 9 (2017) 5683–5691.
[26] M. Zheng, P. Zhao, Z. Luo, et al., ACS Appl. Mater. Interfaces 6 (2014) 6709–6716.
[27] A.L. Antaris, H. Chen, K. Cheng, et al., Nat. Mater. 15 (2016) 235–242.
[28] B. Li, M. Zhao, L. Feng, et al., Nat. Commun. 11 (2020) 3102–3112.
[29] F. Ding, Y. Zhan, X. Lu, Y. Sun, Chem. Sci. 9 (2018) 4370–4380.
[30] S. Wang, Y. Fan, D. Li, et al., Nat. Commun. 10 (2019) 1058–1068.
[31] Z. Feng, X. Yu, M. Jiang, et al., Theranostics 9 (2019) 5706–5719.
[32] T. Li, C. Li, Z. Ruan, et al., ACS Nano 13 (2019) 3691–3702.
[33] X. Peng, F. Song, E. Lu, et al., J. Am. Chem. Soc. 127 (2005) 4170–4171.
[34] G. Xia, Q. Shao, K. Liang, et al., J. Mater. Chem. C 8 (2020) 13621–13626.
[35] H. Bian, D. Ma, X. Zhang, et al., Small 17 (2021) 2100398.
[36] M. Zhou, R. Zhang, M. Huang, et al., J. Am. Chem. Soc. 132 (2010) 15351.